

MARTIN MARIETTA ENERGY SYSTEMS LIBRARIES



3 4456 0334896 4

ORNL/TM-11753

ornl

**OAK RIDGE
NATIONAL
LABORATORY**

MARTIN MARIETTA

Casting of HgCdTe

Part II: Conduction-Diffusion Model and Its Numerical Implementation

Vasilios Alexiades

OAK RIDGE NATIONAL LABORATORY
 CENTRAL RESEARCH LIBRARY
 CIRCULATION SECTION
 ROOM 8009 111
LIBRARY LOAN COPY
 DO NOT TRANSFER TO ANOTHER PERSON
 If you wish someone else to see this
 report, send to same with report and
 the library will arrange a loan.
 OCT 1987 11 11

MANAGED BY
MARTIN MARIETTA ENERGY SYSTEMS, INC.
FOR THE UNITED STATES
DEPARTMENT OF ENERGY

This report has been reproduced directly from the best available copy.

Available to DOE and DOE contractors from the Office of Scientific and Technical Information, P.O. Box 82, Oak Ridge, TN 37831; prices available from (815) 576-8401, FTS 626-8401.

Available to the public from the National Technical Information Service, U.S. Department of Commerce, 5285 Port Royal Rd., Springfield, VA 22161.

This report was prepared as an account of work sponsored by an agency of the United States Government. Neither the United States Government nor any agency thereof, nor any of their employees, makes any warranty, express or implied, or assumes any legal liability or responsibility for the accuracy, completeness, or usefulness of any information, apparatus, product, or process disclosed, or represents that its use would not infringe privately owned rights. Reference herein to any specific commercial product, process, or service by trade name, trademark, manufacturer, or otherwise, does not necessarily constitute or imply its endorsement, recommendation, or favoring by the United States Government or any agency thereof. The views and opinions of authors expressed herein do not necessarily state or reflect those of the United States Government or any agency thereof.

ORNL/TM-11753

Engineering Physics and Mathematics Division
Mathematical Sciences Section

CASTING OF HgCdTe

Part II: Conduction - Diffusion Model and Its Numerical Implementation

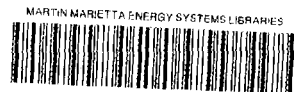
Vasilios Alexiades

Mathematical Sciences Section
Engineering Physics and Mathematics Division
Oak Ridge National Laboratory
Oak Ridge, TN 37831-8083
and
Mathematics Department
University of Tennessee
Knoxville, TN 37996-1300

Date Published: March 1991

Research supported by the Microgravity Science and Applications Division of NASA
under contract H-80582B with the Oak Ridge National Laboratory;
and by the Science Alliance, a Centers of Excellence
program of the State of Tennessee at the University of Tennessee, Knoxville.

Prepared by the
Oak Ridge National Laboratory
Oak Ridge, Tennessee 37831
managed by
MARTIN MARIETTA ENERGY SYSTEMS, INC.
for the
U.S. DEPARTMENT OF ENERGY
under Contract No. DE-AC05-84OR21400



3 4456 0334896 4

TABLE OF CONTENTS

Abstract	1
1. Introduction	1
2. Analytical Model of the Solidification Process	2
2.A Overview	2
2.B Gibbs relation	3
2.C Conservation laws	5
2.D Fluxes	6
2.E Specific energy	8
2.F Heat conduction in the container and in the free space	9
3. Summary of the Model and Algorithm	11
4. Numerical Implementation	11
4.A Numerical grid	11
4.B Discrete conservation laws	12
4.C Discrete fluxes	14
4.D Time-stepping algorithm	15
5. A Numerical Simulation	16
References	22

CASTING OF HgCdTe

Part II: Conduction - Diffusion Model and its Numerical Implementation

Vasilios Alexiades

Mathematics Department
University of Tennessee
Knoxville, Tennessee 37996-1300

and Mathematical Sciences Section
Oak Ridge National Laboratory
Oak Ridge, Tennessee 37831-8083

ABSTRACT

HgCdTe is a technologically important electronic material for which large crystals of uniform composition are desirable. This is very difficult to achieve when the crystal is grown under gravity, so it is important to understand the details of the crystal growth process both qualitatively and quantitatively.

In this report we present the first stage of the effort towards a detailed macroscopic model of the casting process, and its numerical simulation: the basic coupled conduction-diffusion model of the solidification process with constitutional supercooling and its numerical implementation. A compilation of all the relevant thermophysical properties of the pseudo-binary $(\text{HgTe})_{1-x}(\text{CdTe})_x$, as functions of composition x and temperature, is presented in Part I [3]. Simulation experiments will be presented in Part III [4].

1. INTRODUCTION

Mercury-Cadmium-Telluride is a versatile infrared-detector alloy, for which large crystals of uniform composition are desirable. This is very difficult to achieve in any of the bulk crystal growth methods used for its preparation, see [12] for a review. A better quantitative understanding of the crystal growth process is necessary in order to know how the various parameters affect the composition. Modeling and numerical simulation of the casting processes used in its preparation can help us in understanding the details of the process quantitatively, in interpretive experimental measurements, and in designing future earth-bound and microgravity experiments.

A first attempt at quantitative modeling of bulk crystal growth of $\text{Hg}_{1-x}\text{Cd}_x\text{Te}$ from the melt was undertaken in [1], where the solidification of an ingot by convective cooling through a cylindrical quartz ampoule was simulated numerically *in the radial direction only*. The model took into account coupled heat conduction and solute diffusion, constitutional supercooling, the known phase diagram, and thermophysical properties as functions of composition and temperature. A pronounced "skin effect" was observed, namely, a steeply higher solute concentration near the ampoule wall, which matched well the limited experimental measurements available [15]. Sensitivity studies [10], via computational experiments, indicated strong

dependence of the freezing time and of composition on the heat capacity of liquid, which was not known reliably at that time. Subsequently, C.-H. Su [14] derived the dependence of heat capacity, C_P^L , on composition and temperature, directly from the Associated Solution thermodynamic model [6] of the Liquid phase. This information essentially completes the list of property values needed by the model and they are presented in [3], in a form convenient for numerical computations.

The work described here is a natural extension and generalization of our earlier work [1]. We simulate a casting process in *two-dimensions* (r, z coordinates), taking into account conduction in the alloy and the ampoule wall itself, solute diffusion, Soret and Dufour effects, segregation and constitutional supercooling according to the phase diagram, and the presence of a free space inside the ampoule. The model is valid in any number of dimensions, for any binary alloy. It is described in §2, and summarized in §3. Its primitive field variables are only the local concentration (mass fraction of solute) and internal energy, which are being updated directly from the basic conservation laws for mass and energy. All other variables, including temperature, are obtained from the two primitive ones. This new direct approach generalizes the standard, so called "enthalpy method" for moving boundary problems, to alloy solidification. The model is implemented in 2-dimensional (cylindrical) geometry and the numerical scheme is outlined in §4. The Fortran 77 code implementing the scheme for $(HgTe)_{1-x}(CdTe)_x$ incorporates the temperature and composition dependent thermophysical properties described in [3], and it exists in two versions. The serial version runs on any serial-architecture machine (PC, workstation, or a Cray), and the parallel version runs on distributed-memory message-passing parallel machines (such as Intel's hypercubes iPSC/2 and iPSC/860). As illustration, a computational example is presented in §5. Detailed simulation studies will be reported in Part III [4]. The next stage of development of the model will incorporate convection in the melt and an external magnetic field.

2. ANALYTICAL MODEL OF THE SOLIDIFICATION PROCESS

2.A Overview

Mercury-Cadmium-Telluride is viewed as the pseudo-binary $(HgTe)_{1-x}(CdTe)_x$, which, for convenience, we write as $(AC)_{1-x}(BC)_x$, viewing $BC = CdTe$ as the solute. The composition variable, x , represents the *mole fraction* of BC , with corresponding *weight fraction* given by

$$C = \frac{M_{BC} x}{M(x)}, \quad M(x) := M_{AC} (1-x) + M_{BC} x, \quad (2.1a)$$

M_{AC} and M_{BC} being the molecular weights of AC and BC respectively, and $M(x)$ the (formula) molecular weight of the alloy. All property values are expressed as functions of x , but mass conservation is more naturally expressed in terms of C . We will be using both variables, converting one to the other via (2.1) or its inverse

$$x = \frac{M_{AC} C}{M_{AC} C + M_{BC} (1-C)}. \quad (2.1b)$$

In the present model we *exclude* all convective effects by taking the density $\rho^L = \rho^S = \text{constant}$. Such effects will be included in the next version of the model and code. Thus, the alloy solidifies under the simultaneous action of heat conduction and solute diffusion.

The state of the material at location \vec{r} at each time t is characterized by the composition $x(\vec{r}, t)$ (or $C(\vec{r}, t)$) and temperature $T(\vec{r}, t)$, with the phase (liquid, solid, or "mushy") being determined from the (pseudo binary) phase diagram, shown in Figure 1, (we assume that conditions of local thermodynamic equilibrium prevail throughout the process). The liquidus and solidus curves of the phase diagram are monotone curves which may be represented, respectively, by the equations

$$x = x^L(T) \quad \text{and} \quad x = x^S(T), \quad (2.2a)$$

or, equivalently, by their inverses

$$T = T^L(x) \quad \text{and} \quad T = T^S(x) \quad (2.2b)$$

(see Part I, §2, for expressions representing these functions). These two curves demarcate three possible phases: *Liquid* above the liquidus curve, *solid* below the solidus curve, and a two-phase coexistence region of constitutionally supercooled alloy, which we shall be referring to as "*mushy*".

The *internal energy* at state (x, T) , which coincides with the enthalpy here (due to $\rho \equiv \text{constant}$), will be denoted by $E(x, T)$, and its value per gram by $e(x, T) = \text{specific energy}$. We shall follow the convention of using upper case letters for *molar* quantities (E, \bar{H}, C_p) and lower case letters for their *specific* values (e, \bar{h}, c_p). Mole fractions and molar units are natural for thermodynamic considerations and properties, whereas conservation laws are more naturally expressed in terms of mass fractions, on a per gram basis.

2.B Gibbs relation

Within each pure phase (liquid and solid), the (integral) molar energy (enthalpy) $E(x, T)$ at state (x, T) is determined from the Gibbs relation

$$dE^j(x, T) = \bar{H}^j dx + C_p^j dT, \quad j = L, S, sp \quad (2.3)$$

by integration over any convenient path on the phase diagram (see §2.D). Here

$$\bar{H}^j(x, T) := \bar{H}_{BC}^j - \bar{H}_{AC}^j, \quad \bar{H}_i^j(x, T) = \text{partial molar enthalpy of species } i = AC, BC, \\ \text{in phase } j = L, S,$$

and

$$C_p^j(x, T) = \text{molar heat capacity of the alloy in phase } j = L, S.$$

When the state (x, T) is mushy (i.e. $x^L(T) < x < x^S(T)$), then the material is a mixture of Liquid at state $(x^L(T), T)$ and Solid at state $(x^S(T), T)$, which coexist in equilibrium at temperature T , in proportions determined by the local liquid fraction $\lambda(x, T)$. According to the lever rule,

HgTe - CdTe Phase Diagram

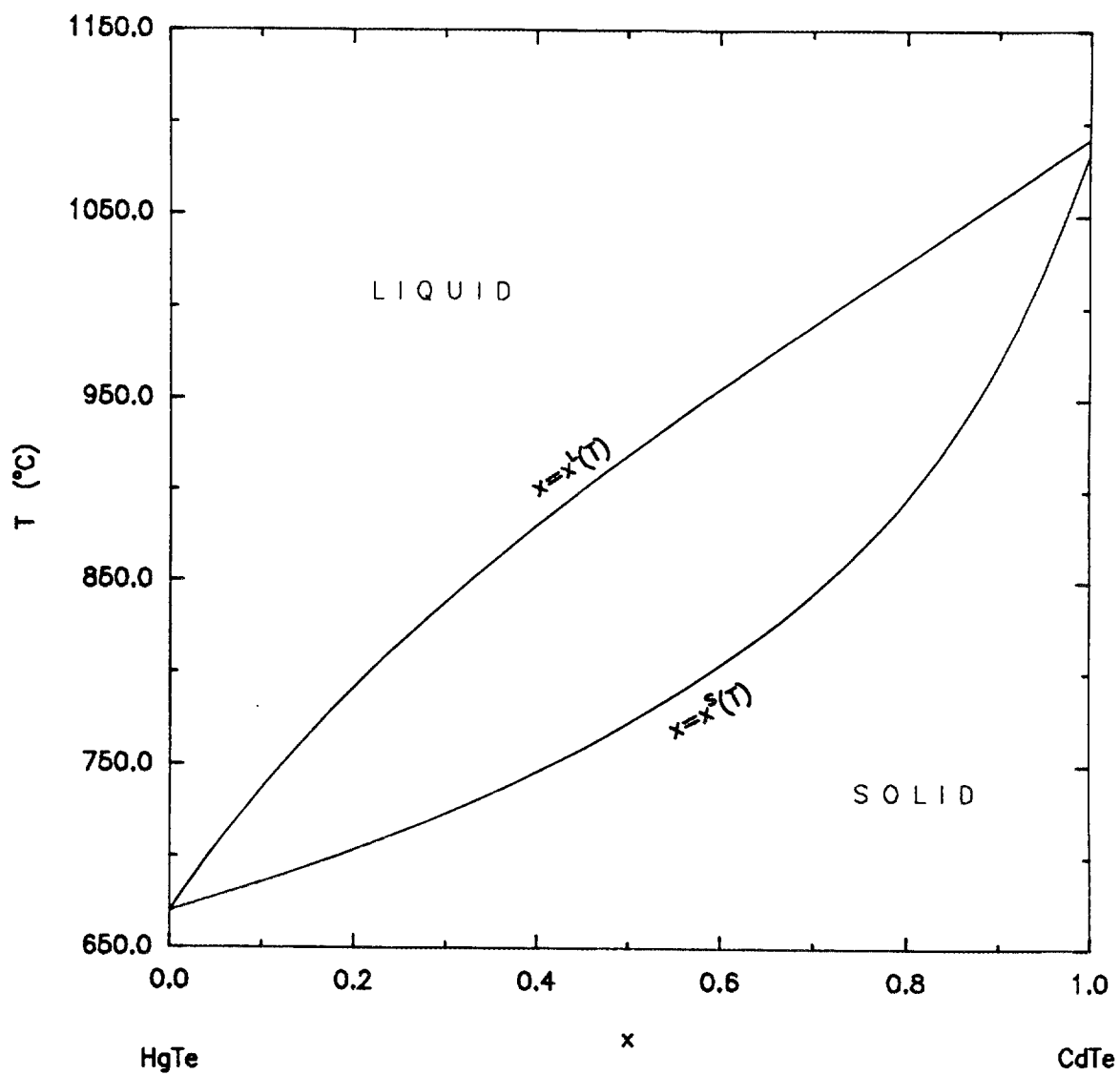


Figure 1

$$\lambda(x, T) = \frac{x^S(T) - x}{x^S(T) - x^L(T)}, \quad x^L(T) < x < x^S(T), \quad (2.4)$$

and

$$E^m(x, T) = \lambda(x, T) E^L(x^L(T), T) + [1 - \lambda(x, T)] E^S(x^S(T), T), \quad (2.5)$$

in the mushy case. Note that for fixed x , $E^j(x, T)$ is an increasing function of T within each phase $j = L, m, S$, which will allow us to determine T from knowing x and E .

2.C Conservation Laws

The diffusion of solute ($BC = CdTe$) and conduction of heat are governed by the conservation laws

$$\rho C_t + \text{div } \vec{j} = 0, \quad (2.6)$$

$$\rho e_t + \text{div } \vec{q} = 0, \quad (2.7)$$

where ρ = density (\equiv constant), C = mass fraction of BC , \vec{j} = mass flux of BC , $e(C, T)$ = specific internal energy (or enthalpy here) at state (C, T) and \vec{q} = energy flux. The constitutive laws relating fluxes with fields ([16], [5]; see [2] for details) are

$$\text{Fick's Law:} \quad \vec{j} = -\rho D \nabla C + \rho \delta \nabla T, \quad (2.8)$$

$$\text{Fourier's Law:} \quad \vec{G} = -k \nabla T + \beta \nabla C, \quad (2.9)$$

and

$$\vec{q} = \vec{G} + \bar{h} \vec{j}, \quad (2.10)$$

where D = material diffusivity, \vec{G} = heat flux, k = thermal conductivity, and $\bar{h} = \bar{h}_{BC} - \bar{h}_{AC}$ = difference of the partial specific enthalpies \bar{h}_i of species $i = BC, AC$. In (2.8), (2.9) we have also included thermo-diffusion cross effects, with δ and β denoting the Soret and Dufour coefficients; these are usually thought to be negligibly small, and no experimental measurements exist for them. We retain them in the model in order to be able to study their contribution on the overall process via numerical experiments, by comparison with the case $\delta = \beta = 0$. Note that $\delta > 0$ in (2.8) would imply that solute diffuses towards the hotter region.

The conservation laws are valid globally, irrespectively of phase, and they determine the evolution of the system over time. However, since the fields and fluxes are not necessarily smooth (differentiable), the laws must be interpreted in a weak sense and *not* pointwise. Such mathematically valid interpretations are available via the modern theory of partial differential equations (see, e.g., [8], [9]). For our purposes here, it is sufficient to interpret them in their most primitive physical sense, namely integrated over any (control) volume and time interval $[t, t + \Delta t]$:

$$\int_V \rho C(\vec{r}, t + \Delta t) dV - \int_V \rho C(\vec{r}, t) dV + \Delta t \int_t^{t+\Delta t} \int_A \vec{j} \cdot \vec{n} dA d\tau = 0 \quad (2.6)^*$$

$$\int_V \rho e(\vec{r}, t + \Delta t) dV - \int_V \rho e(\vec{r}, t) dV + \Delta t \int_t^{t+\Delta t} \int_A \vec{q} \cdot \vec{n} dA d\tau = 0 \quad (2.7)^*$$

where \vec{n} denotes the outgoing normal to the boundary A of the control volume V . Our numerical scheme will be based on these.

They can be used directly to *update* the mean concentration $C(\vec{r}, t + \Delta t)$ and energy $e(\vec{r}, t + \Delta t)$ to a new time $t + \Delta t$ from values of C and T at an earlier time t , for each location \vec{r} . Then, knowing C and e at the new time we need to update the temperature T to the new time. To do this, we must know the new phase. Fortunately, the pair (C, e) does determine the phase uniquely, and the monotonicity of $e(C, T)$ as function of T , for fixed C , allows us to solve for T (see §2.C). The standard alternative to this new direct approach is to eliminate e from the system (2.6)-(2.7) using Gibbs relations, in favor of C and T , as was done in [1]. In the absence of phase-changes, elimination of e would be preferable since e and T are simply related by $de = c_p dT$ and e conveys no more information than T does. For phase-change processes however, these two variables are *not* equivalent; the temperature cannot distinguish solid from liquid at the melt temperature, only the enthalpy can, since it experiences a jump there, equal to the heat of fusion (latent heat). This observation constitutes the basis of the so-called ‘‘enthalpy method’’ for Stefan-type problems [8]. Thus, the direct approach to conservation laws we employ here generalizes the ‘‘enthalpy method’’ to alloy solidification.

2.D Fluxes

Having interpreted the basic conservation laws in their primitive integral sense, we also need to make precise the constitutive laws for fluxes in a mushy (two-phase) volume. Let us first discuss the *diffusion flux* $\vec{J} := -D \nabla C$ in a mushy volume V having liquid fraction λ , mean concentration C and mean temperature T . To the temperature T there correspond the liquidus and solidus compositions $x^L(T)$ and $x^S(T)$ from the phase diagram (see (2.2)). Convert them to weight fractions via (2.1), and call them $C^L(T)$ and $C^S(T)$. In fact, it is convenient to extend their definitions to include $\lambda = 0$ and $\lambda = 1$, as follows:

$$C^L(T) := \begin{cases} 0 & \text{if } \lambda = 0 \\ \frac{M_{BC} x^L(T)}{M(x^L(T))} & \text{if } 0 < \lambda < 1 \\ C & \text{if } \lambda = 1 \end{cases}, \quad C^S(T) := \begin{cases} C & \text{if } \lambda = 0 \\ \frac{M_{BC} x^S(T)}{M(x^S(T))} & \text{if } 0 < \lambda < 1 \\ 0 & \text{if } \lambda = 1, \end{cases} \quad (2.11)$$

where $M(x)$ is the formula weight (see (2.1)). Define the corresponding liquid fraction

$$\Lambda(C, T) := \frac{C^S(T) - C}{C^S(T) - C^L(T)} \quad (2.12)$$

(equivalently, $\Lambda = \frac{M(x^L)}{M(x)} \lambda$, so for solid: $\Lambda = 0 = \lambda$ and for liquid $\Lambda = 1 = \lambda$), so that the lever rule:

$$C = \Lambda C^L(T) + [1 - \Lambda] C^S(T) \quad (2.13)$$

is valid for all $0 \leq \Lambda \leq 1$. In the liquid (portion), the diffusion flux is $\vec{J}^L := -D^L \nabla C^L$ and in the solid (portion) $\vec{J}^S := -D^S \nabla C^S$, so the total flux will be

$$\vec{J} = \Lambda(-D^L \nabla C^L) + [1 - \Lambda](-D^S \nabla C^S) . \quad (2.14)$$

Clearly, if the volume is all liquid then $\Lambda = 1$, $C^L = C$, $C^S = 0$ so (2.14) gives $\vec{J} = -D^L \nabla C$; and if all solid then $\Lambda = 0$, $C^L = 0$, $C^S = C$, so (2.14) gives $\vec{J} = -D^S \nabla C$. The important aspect is that diffusion in the mushy case is driven by gradients of the liquidus and solidus concentrations only (and *not* by gradients in mean concentration). Note that C^L and C^S depend *only* on temperature, so whenever the temperature is uniform, C^L and C^S will also be uniform, their gradients will be zero, and there will be no Fickian diffusion, even if the mean concentration is non-uniform. Numerical approximation to the diffusive flux will be described in §4.B.

Next, we consider Fourier's law, $\vec{G} = -k \nabla T$, for a mushy volume V of liquid fraction λ , and mean temperature T . We may define different effective conductivities in the various coordinate directions, so let us discuss the flux component $G = -k \frac{\partial T}{\partial r}$, in a generic direction r , for definiteness. There are several "mixture" rules for effective conductivities [7], based on steady-state considerations and depending on what "layer structure" one assumes existing in the mixture. They range from the "serial arrangement" to "parallel arrangement" and various rules interpolating these two extremes.

If we assume a columnar type structure normal to the r -direction, (serial arrangement) then the resistivity to conduction through liquid will be $\frac{\lambda}{k^L}$ and through solid $\frac{1-\lambda}{k^S}$; the total resistivity will then be

$$\frac{1}{k} = \frac{\lambda}{k^L} + \frac{1-\lambda}{k^S} . \quad (2.15)$$

On the other hand, if we assume layers parallel to the r -direction, then the conductivities add up, and the effective conductivity will be

$$k = \lambda k^L + (1 - \lambda) k^S . \quad (2.16)$$

Neither one of these is appropriate for an amorphous mixture of solid and liquid, in which case we may use the formula [7, p. 242]

$$k = k^S \frac{1 + \lambda^{2/3} (\kappa - 1)}{1 + (\lambda^{2/3} - \lambda) (\kappa - 1)}, \quad \kappa = \frac{k^L}{k^S}, \quad (2.17)$$

which interpolates the two previous ones.

2.E Specific energy

The Gibbs relation (2.3) on a per gram basis has the form

$$de^j(C, T) = \bar{h}^j dC + c_p^j dT, \quad j = L, S$$

where $\bar{h}^j := \bar{h}_{BC}^j - \bar{h}_{AC}^j$, \bar{h}_i^j = partial *specific enthalpy* (cal/g) of $i = AC, BC$ in phase $j = L, S$, and c_p^j = specific heat (cal/g K). From $C = \frac{M_{BC}}{M(x)} x$ (see (2.1)), we get $dC = \frac{M_{AC} M_{BC}}{M(x)^2} dx$, whence

$$de^j(x, T) = \bar{h}^j(x, T) dx + c_p^j(x, T) dT, \quad j = L, S \quad (2.18)$$

with $\bar{h}^j := \bar{h}^j \frac{M_{AC} M_{BC}}{M(x)^2}$.

As reference state (of zero energy) we choose pure AC ($x = 0$) *solid* at its melt temperature T_{AC} , and write the energy as:

$$e(x, T) = \begin{cases} e^S(x, T) := \int_0^x \bar{h}^S(y, T_{AC}) dy + \int_{T_{AC}}^T c_p^S(x, \tau) d\tau, & \text{if } T \leq T^S(x) \text{ (solid),} \\ e^m(x, T) := \lambda(x, T) e^L(x^L(T), T) + [1 - \lambda(x, T)] e^S(x^S(T), T), & \text{if } T^S(x) < T < T^L(x), \text{ (mushy)} \\ e^L(x, T) := \Delta e_{AC}(T_{AC}) + \int_{T_{AC}}^T c_p^L(0, \tau) d\tau + \int_0^x \bar{h}^L(y, T) dy, & \text{if } T \geq T^L(x) \text{ (liquid),} \end{cases} \quad (2.19)$$

where Δe_{AC} = heat of fusion of pure AC at its melt temperature T_{AC} .

In particular, the energies at $(x, T^S(x))$ and $(x, T^L(x))$ depend *only* on x . Therefore, given x , we can compute the two values:

$$e^S(x) := e^S(x, T^S(x)) = \int_0^x \bar{h}^S(y, T_{AC}) dy + \int_{T_{AC}}^{T^S(x)} c_p^S(x, \tau) d\tau \quad (2.20)$$

and

$$e^L(x) := e^L(x, T^L(x)) = \Delta e_{AC} + \int_{T_{AC}}^{T^L(x)} c_p^L(0, \tau) d\tau + \int_0^x \bar{h}^L(y, T^L(x)) dy, \quad (2.21)$$

and $e(x, T)$ can be expressed as

$$e(x, T) = \begin{cases} e^S(x, T) = \varepsilon^S(x) + \int_{T^S(x)}^T c_p^S(x, \tau) d\tau, & \text{if } T \leq T^S(x) \text{ (solid)} \\ e^m(x, T) = \lambda(x, T) e^L(x^L(T), T) + [1 - \lambda(x, T)] e^S(x^S(T), T), & \text{if } T^S(x) < T < T^L(x) \text{ (mushy)} \\ e^L(x, T) = \varepsilon^L(x) + \int_{T^L(x)}^T c_p^L(x, \tau) d\tau, & \text{if } T \geq T^L(x) \text{ (liquid)} \end{cases} \quad (2.22)$$

Since, for solid, $e \leq \varepsilon^S(x)$ and for liquid $e \geq \varepsilon^L(x)$, we see that the pair (x, e) characterizes the phases as well as the pair (x, T) does.

We conclude that, given the numbers x and e ,

if $e \leq \varepsilon^S(x)$ then the phase is **solid** and T can be found by solving the equation

$$\varepsilon^S(x) + \int_{T^S(x)}^T c_p^S(x, \tau) d\tau = e; \quad (2.23)_S$$

if $\varepsilon^S(x) < e < \varepsilon^L(x)$ then the phase is **mushy** and T can be found from

$$\lambda(x, T) e^L(x^L(T), T) + [1 - \lambda(x, T)] e^S(x^S(T), T) = e; \quad (2.23)_m$$

if $\varepsilon^L(x) \leq e$ then the phase is **liquid** and T can be found from

$$\varepsilon^L(x) + \int_{T^L(x)}^T c_p^L(x, \tau) d\tau = e. \quad (2.23)_L$$

Even though the equation: $e^m(x, T) = e$ for T in the mushy case is complicated, it is easy to see that it has a solution T between $T^S(x)$ and $T^L(x)$. Indeed, at $T = T^S(x)$ we have $\lambda = 0$ (because $x^S(T^S(x)) - x = x - x = 0$, since $T^S(x)$ is the inverse function to $x^S(T)$), and $e^S(x^S(T^S(x)), T^S(x)) = e^S(x, T^S(x)) \equiv \varepsilon^S(x) < e$; on the other hand, at $T = T^L(x)$, we have $\lambda = 1$ and $e^L(x^L(T^L(x)), T^L(x)) = e^L(x, T^L(x)) \equiv \varepsilon^L(x) > e$; hence the expression $e^m(x, T) - e$ changes sign on the interval $[T^S(x), T^L(x)]$, and it is easy to solve by a bisection type method (e.g. Brent's method, [13]).

2.F Heat conduction in the container and in the free space

Heat conduction in the container's walls may be conveniently incorporated into the same energy updating scheme.

Conservation of energy in the wall is governed by

$$\rho^w e_t^w + \text{div} \vec{q}^w = 0 \quad (2.24)$$

where $\rho^w =$ density (\equiv const.), $e^w(T) =$ specific internal energy (enthalpy) at temperature $T(\vec{r}, t)$ at location \vec{r} in the wall at time t , and

$$\vec{q}^w = -k^w \nabla T = \text{conductive flux in the wall} \quad (2.25)$$

with k^w the thermal conductivity of the wall. Since the Gibbs relation here is

$$de^w = c_p^w dT, \quad (2.26)$$

with c_p^w = specific heat of the wall material, (2.24) is simply the primitive form of the standard heat conduction equation

$$\rho^w c_p^w T_t - \text{div}(k^w \nabla T) = 0.$$

Knowing the temperature field at time t , we use (2.24) to update e^w to a later time $t + \Delta t$ and then update the temperature from (2.26). If c_p^w is a constant, this is simply

$$T = T_{AC} + \frac{e^w}{c_p^w} \quad (2.27)$$

(using T_{AC} as reference temperature, where $e^w = 0$). More generally, if c_p^w varies with temperature, then we must solve for T the equation

$$\int_{T_{AC}}^T c_p^w(\tau) d\tau = e^w \quad (2.28)$$

(analogous to (2.23)). It is uniquely solvable since $c_p^w > 0$ implies the left-hand side is strictly increasing function of T .

The free (void) space inside the ampoule is filled with vapor of Mercury whose pressure and density are functions of temperature. Since this density is at least two orders of magnitude lower than the density of the alloy, we may consider the mass (hence also the energy) in the void space as negligible. Then this space is simply a thermal layer at a uniform temperature T^{void} responding to the temperature of the surroundings with conductivity k^{vapor} . The heat conduction equation now reduces to

$$0 = \text{div } q^{\text{void}}, \quad (2.29)$$

which, upon integration over the void, simply says that the sum of the fluxes along the boundary of the void is zero. Hence, at each time, T^{void} is a weighted average of the surrounding temperatures and may be found easily.

3. SUMMARY OF THE MODEL AND ALGORITHM

The primary unknowns are the temperature and concentration fields as they evolve in time, namely $T(\vec{r}, t)$ and $x(\vec{r}, t)$ (or $C(\vec{r}, t)$, via (2.1)). They are determined from the conservation laws (2.6)-(2.10), (2.24)-(2.25), (2.29) and the relations (2.23), (2.28).

Let's describe the basic steps of the algorithm. The data of the problem are:

- thermophysical properties of the alloy: ρ (\equiv constant here), $c_p^L(x, T)$, $c_p^S(x, T)$, $\bar{h}^L(x, T)$, $\bar{h}^S(x, T)$,
 $k^L(x, T)$, $k^S(x, T)$, D^L , D^S , δ^L , δ^S , β^L , β^S ;
- phase diagram: $x = x^L(T)$, $x = x^S(T)$;
- thermophysical properties of the container: ρ^w , c_p^w , k^w ; and of the vapor filling the void: k^{vapor} ;
- initial temperature and composition: $T(\vec{r}, 0)$, $x(\vec{r}, 0)$;
- boundary conditions on the outer surface of the container, (e.g. the temperature imposed there), and zero mass-flux at the inner (cavity) walls.

We update the energy e from (2.24) in the walls (using the boundary conditions) and from (2.7) in the alloy, and also update C from (2.6). Convert C to x via (2.1b), and update T from (2.23) in the alloy, from (2.28) in the walls, and from (2.29) in the free space. Thus we find e , C , x and T at the new time, and can proceed to the next time step.

Clearly, the model and algorithm are valid in any number of dimensions, for any binary alloy. The only restriction is the exclusion of convective effects which can naturally be incorporated into the overall scheme by adding momentum conservation for the velocity field and the appropriate convective terms in the mass and energy conservations laws. This will be done in the next version of the model and code.

4. NUMERICAL IMPLEMENTATION

We consider axisymmetric solidification in a cylindrical mold of inner radius R_{in} , outer radius R_{out} , inner height Z_{in} and outer height $Z_{in} + Z_{void} + 2Z_w$, Z_w being the thickness of the top and bottom walls, and Z_{void} the height of the void space (filled with Hg vapor). For simplicity in the presentation we neglect the void and only describe the case $Z_{void} = 0$ here.

4.A Numerical grid

Given four integers I_p, I_w, J_p, J_w , let

$$\Delta r = R_{in}/I_p, \quad \Delta r_w = (R_{out} - R_{in})/I_w, \quad \Delta z = Z_{in}/J_p, \quad \Delta z_w = Z_w/J_w$$

and set up the mesh shown in Figure 2. The indices range as follows: for nodes

$$\begin{aligned} r_i : i = 1, \dots, I_p, (\text{cavity}); \quad i = I_p + 1, \dots, I_p + I_w (\text{wall}); \\ z_j : j = 1, \dots, J_p (\text{cavity}); \quad j = -J_w + 1, \dots, 0 (\text{bottom wall}); \quad j = J_p + 1, \dots, J_p + J_w (\text{top wall}); \end{aligned}$$

and for faces:

where Δe_{AC} = heat of fusion of pure AC at its melt

$$\begin{aligned} R_{i-\frac{1}{2}} : i = 1, \dots, I_p + 1 (\text{cavity}); \quad i = I_p + 1, \dots, I_p + I_w + 1 (\text{wall}) \\ (r_{\frac{1}{2}} = 0, \quad r_{I_p + \frac{1}{2}} = R_{in}, \quad r_{I_p + I_w + \frac{1}{2}} = R_{out}) \\ z_{j-\frac{1}{2}} : j = 1, \dots, J_p + 1 (\text{cavity}); \quad j = -J_w + 1, \dots, 1 (\text{bottom wall}); \quad j = J_p + 1, \dots, J_p + J_w + 1 (\text{top wall}) \\ (z_{-J_w + \frac{1}{2}} = -Z_w, \quad z_{\frac{1}{2}} = 0, \quad z_{J_p + \frac{1}{2}} = Z_{in}, \quad z_{J_p + J_w + \frac{1}{2}} = Z_{in} + Z_w) \end{aligned}$$

The ij -th control volume is centered at (r_i, z_j) and has volume (of revolution)

$$V_{ij} = \pi[r_{i+\frac{1}{2}}^2 - r_{i-\frac{1}{2}}^2][z_{j+\frac{1}{2}} - z_{j-\frac{1}{2}}], \quad \begin{aligned} i = 1, \dots, I_p, I_p + 1, \dots, I_p + I_w \\ j = -J_w + 1, \dots, 0, 1, \dots, J_p, J_p + 1, \dots, J_p + J_w \end{aligned}$$

The area of a radial face is

$$A_{i-\frac{1}{2},j} = 2\pi r_{i-\frac{1}{2}}[z_{j+\frac{1}{2}} - z_{j-\frac{1}{2}}], \quad \begin{aligned} i = 1, \dots, I_p, I_p + 1, \dots, I_p + I_w + 1 \\ j = -J_w + 1, \dots, J_p + J_w \end{aligned}$$

and of an axial face

$$A_{i,j-\frac{1}{2}} = \pi[r_{i+\frac{1}{2}}^2 - r_{i-\frac{1}{2}}^2], \quad \begin{aligned} i = 1, \dots, I_p + I_w \\ j = -J_w + 1, \dots, 0, 1, \dots, J_p, J_p + 1, \dots, J_p + J_w + 1 \end{aligned}$$

The field variables e, C, x, λ, T will be represented discretely by their mean values, $e_{ij}^n, C_{ij}^n, x_{ij}^n, \lambda_{ij}^n, T_{ij}^n$, over the control volume V_{ij} , at time t_n , and they will be associated with the node (r_i, z_j) .

4.B Discrete conservation laws

We integrate (2.6), (2.7) over each control volume V_{ij} and over a time step $[t_n, t_{n+1}]$ of length $\Delta t_n = t_{n+1} - t_n$, i.e. use (2.6)*, (2.7)* for each V_{ij} . Denoting by C_{ij}^n and e_{ij}^n the mean values of C and e over V_{ij} at time t_n , by $AJ_{i\pm\frac{1}{2},j}^n, AJ_{i,j\pm\frac{1}{2}}^n$, the mass flow rates and by $AQ_{i\pm\frac{1}{2},j}^n, AQ_{i,j\pm\frac{1}{2}}^n$ the energy flow rates (area \times flux) through the radial faces ($A_{i\pm\frac{1}{2},j}$) and axial faces ($A_{i,j\pm\frac{1}{2}}$), we obtain the forward Euler (explicit in time) discrete mass and energy balance equations:

$$\begin{aligned} C_{ij}^{n+1} = C_{ij}^n + \frac{\Delta t_n}{V_{ij}} \{AJ_{i-\frac{1}{2},j}^n - AJ_{i+\frac{1}{2},j}^n + AJ_{i,j-\frac{1}{2}}^n - AJ_{i,j+\frac{1}{2}}^n\} \\ i = 1, \dots, I_p, j = 1, \dots, J_p \end{aligned} \quad (4.1)$$

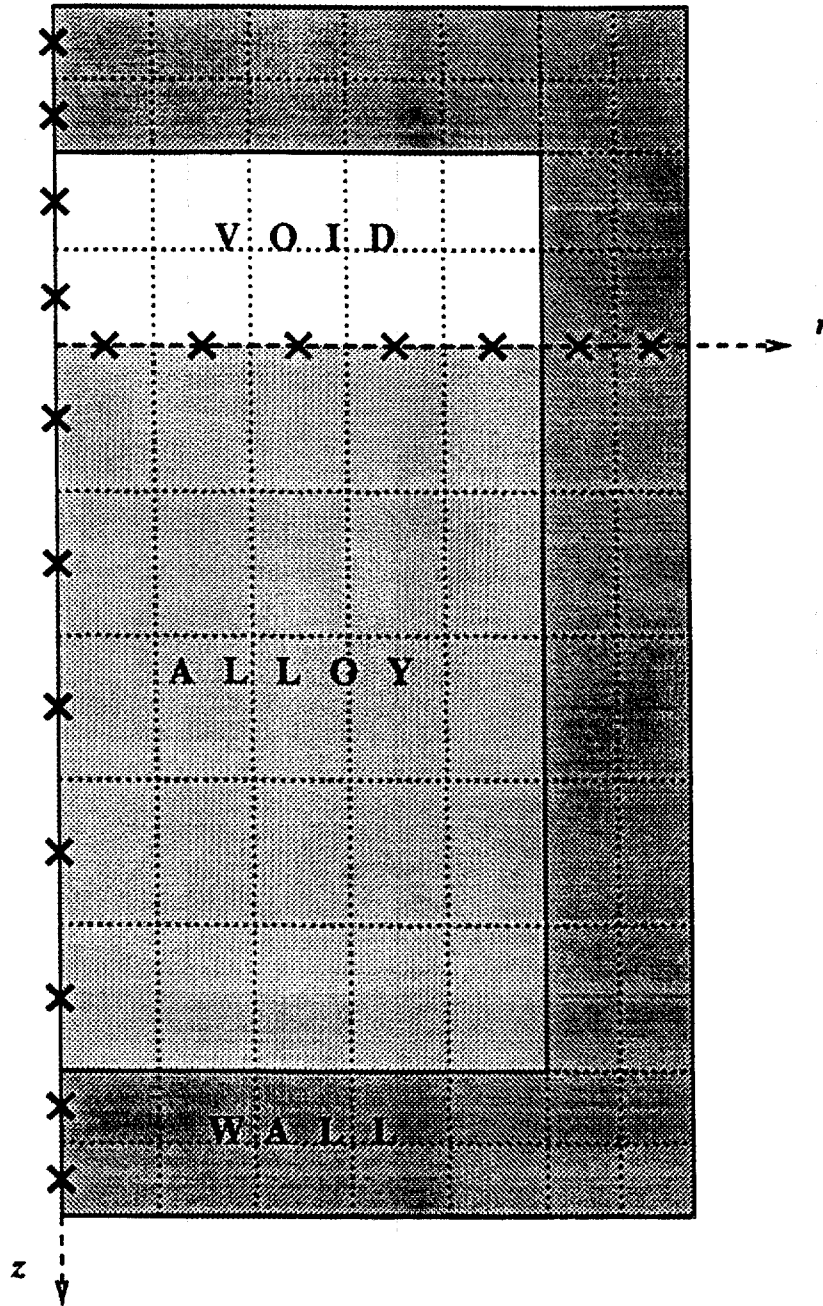


Figure 2. Representative control volumes

$$e_{ij}^{n+1} = e_{ij}^n + \frac{\Delta t_n}{V_{ij}} \{AQ_{i-1/2,j}^n - AQ_{i+1/2,j}^n + AQ_{i,j-1/2}^n - AQ_{i,j+1/2}^n\} \quad (4.2)$$

$$i = 1, \dots, J_p, J_p+1, \dots, J_p+J_w, \quad j = -J_w+1, \dots, 0, 1, \dots, J_p, \dots, J_p+J_w$$

The time steps Δt_n , $n = 0, 1, \dots$, are chosen from a Courant-Friedricks-Levy (CFL) condition to ensure numerical stability of the explicit scheme.

The reasons we prefer to use an explicit scheme over an implicit one are twofold. First, implicit schemes are only marginally more efficient for highly nonlinear phase-change problems. Their time step may be taken a few times larger than the explicit one, but the number of iterations required for convergence is of the same order as this factor. Given the added programming and computations the implicit scheme requires, the net gain is at best marginal. The second and principal reason is that recent experience, [11], has shown the explicit scheme to be more efficient for parallel distributed memory (message-passing) computers, such as the Intel iPSC/860 hypercube on which most of the fine-mesh runs are to be performed.

4.C Discrete fluxes

We need expressions for the discrete flow rates appearing in (4.1), (4.2). Consider any two adjacent control volumes V_1 and V_2 , say in the r -direction, with common face A and radial distance (between their nodes) Δr . Let λ_1, λ_2 ; C_1, C_2 ; T_1, T_2 be their liquid fractions, mean concentrations and mean temperatures, and Λ_1, Λ_2 ; $C_1^L, C_2^L, C_1^S, C_2^S$ the quantities defined by (2.11), (2.12).

Keeping in mind the discussion in §2.3, the (radial) mass flow rate AJ normal to the face of area A is taken to be

$$AJ_{1+1/2} = -A \cdot \left[\min\{\Lambda_1, \Lambda_2\} D^L \frac{C_2^L - C_1^L}{\Delta r} + \left[1 - \min\{\Lambda_1, \Lambda_2\} \right] D^S \frac{C_2^S - C_1^S}{\Delta r} - \delta \frac{T_2 - T_1}{\Delta r} \right]. \quad (4.3)$$

This allows diffusion between the liquid portions (across the area $A \cdot \min\{\Lambda_1, \Lambda_2\}$) of the volumes, and between their solid portions (across an area $A \cdot (1 - \min\{\Lambda_1, \Lambda_2\})$). For the Soret coefficient we have taken $\delta^L = \delta^S =: \delta$, for simplicity. A similar formula may be used for flow rates in the z -direction.

For the heat flux (2.9), we implement the resistivity method (2.15) to compute an effective resistivity

$$R_{eff} = \frac{\lambda}{k^L} + \frac{1-\lambda}{k^S} \quad (4.4)$$

for each node in the alloy, while $R_{eff} = 1/k^w$ for wall nodes (and $R_{eff} = 1/k^{vapor}$ for void nodes).

Letting r_1, r_2 denote the r -locations of the nodes of V_1, V_2 ($r_2 - r_1 = \Delta r$) and $r_{1+1/2}$ the r -location of the common face between them, $r_1 < r_{1+1/2} < r_2$, the total resistance to heat flow from r_1 to r_2 is

$$R = [r_{1+\frac{1}{2}} - r_1]R_{eff_1} + [r_2 - r_{1+\frac{1}{2}}]R_{eff_2} . \quad (4.5)$$

Thus the discrete version of the heat flux, (2.9), taking $\beta^L = \beta^S =: \beta$, is

$$G_{1+\frac{1}{2}} = -\frac{T_2 - T_1}{R} + \beta \frac{C_2 - C_1}{\Delta r} , \quad (4.6)$$

and the energy flow-rate across the face of area A is taken to be

$$(AQ)_{1+\frac{1}{2}} := A \cdot G_{1+\frac{1}{2}} + (AJ)_{1+\frac{1}{2}} \cdot \rho \cdot \frac{\bar{h}_1 + \bar{h}_2}{2} , \quad (4.7)$$

where we have used a simple averaging of the nodal values \bar{h}_1, \bar{h}_2 , to approximate the value of \bar{h} at the midpoint $r_{1+\frac{1}{2}}$, and $(AJ)_{1+\frac{1}{2}}$ is from (4.3). A similar formula may be used in the z -direction. Inside the walls, (4.7) reduces simply to $AQ = A \cdot (-k^w \frac{T_2 - T_1}{\Delta r})$.

4.D Time-stepping algorithm

With each control volume V_{ij} , whose node is at (r_i, z_j) , we associate the following discrete quantities (superscript n denotes value at time t_n):

V_{ij} (volume); $A_{i\pm\frac{1}{2}j}, A_{ij\pm\frac{1}{2}}$ (areas of radial and axial faces);

e_{ij}^n (mean specific energy); T_{ij}^n (temperature);

λ_{ij}^n (liquid fraction); C_{ij}^n (mean concentration); CL_{ij}^n, CS_{ij}^n (see (2.11));

x_{ij}^n (mean composition); c_{pij}^n (mean specific heat); \bar{h}_{ij}^n (mean specific enthalpy difference);

$Reff_{ij}^n$ (effective resistivity);

$AJ_{i\pm\frac{1}{2}j}^n, AJ_{ij\pm\frac{1}{2}}^n$ (mass flow rates across the corresponding faces);

$AQ_{i\pm\frac{1}{2}j}^n, AQ_{ij\pm\frac{1}{2}}^n$ (energy flow rates).

Knowing $e_{ij}^n, T_{ij}^n, \lambda_{ij}^n, C_{ij}^n, CL_{ij}^n, CS_{ij}^n, x_{ij}^n$ at time t_n , their updating to time $t_{n+1} = t_n + \Delta t_n$ proceeds as follows:

Step 1: Evaluate the conductivities $k^L(x_{ij}^n, T_{ij}^n), k^S(x_{ij}^n, T_{ij}^n)$, also

$$\begin{aligned} \bar{h}_{ij}^n &= \lambda_{ij}^n \bar{h}^L(x_{ij}^n, T_{ij}^n) + (1 - \lambda_{ij}^n) \bar{h}^S(x_{ij}^n, T_{ij}^n), \\ c_{pij}^n &= \lambda_{ij}^n c_p^L(x_{ij}^n, T_{ij}^n) + [1 - \lambda_{ij}^n] c_p^S(x_{ij}^n, T_{ij}^n). \end{aligned} \quad \text{and}$$

Compute $Reff_{ij}^n$ from (4.4), and the allowable time-step Δt_n from a numerical stability (CFL) criterion. Set time = $t_n + \Delta t_n$.

Step 2: Compute the flow rates $AJ_{i\pm\frac{1}{2}j}^n, AJ_{ij\pm\frac{1}{2}}^n, AQ_{i\pm\frac{1}{2}j}^n, AQ_{ij\pm\frac{1}{2}}^n$ from (4.3), (4.7).

- Step 3:** Compute C_{ij}^{n+1} and e_{ij}^{n+1} from (4.1) and (4.2).
- Step 4:** Find x_{ij}^{n+1} from (2.1b), and compute the quantities $\epsilon^S(x_{ij}^{n+1})$, $\epsilon^L(x_{ij}^{n+1})$ from (2.20), (2.21). According to (2.23),
- if $e_{ij}^{n+1} \leq \epsilon^S(x_{ij}^{n+1})$ then set $\lambda_{ij}^{n+1} = 0$, $CL_{ij}^{n+1} = 0$, $CS_{ij}^{n+1} = C_{ij}^{n+1}$
and find T_{ij}^{n+1} by solving (2.23)_S;
- if $\epsilon^S(x_{ij}^{n+1}) < e_{ij}^{n+1} < \epsilon^L(x_{ij}^{n+1})$ then find λ_{ij}^{n+1} from (2.4),
 CL_{ij}^{n+1} and CS_{ij}^{n+1} from (2.11), and T_{ij}^{n+1} by solving (2.23)_m;
- if $\epsilon^L(x_{ij}^{n+1}) \leq e_{ij}^{n+1}$ then set $\lambda_{ij}^{n+1} = 1$, $CL_{ij}^{n+1} = C_{ij}^{n+1}$, $CS_{ij}^{n+1} = 0$,
and find T_{ij}^{n+1} by solving (2.23)_L.

Thus all the field quantities are updated to the new time $t_{n+1} = t_n + \Delta t_n$. Of course, for wall nodes T_{ij}^{n+1} is directly found from (2.28). As for T^{void} , it is obtained as a weighted average (derived from (2.29)) of the nodal temperatures surrounding the void.

5. A NUMERICAL SIMULATION

Consider a quartz ampoule of inner radius $R_{in} = 0.5 \text{ cm}$, height $Z_{in} = 9 \text{ cm}$, and wall thickness $Z_w = 0.3 \text{ cm}$. It is filled entirely (no free space) with $HgCdTe$ of uniform composition $x_{inü} = 0.2$ and initially the system is at uniform temperature $T_{inü} = 820^\circ\text{C}$, so the alloy is in its liquid phase. At time $t = 0$, we impose a constant temperature $T_{bry} = 650^\circ\text{C}$ at the outer surface of the cylinder and let it solidify.

We have simulated this casting process using 20×128 nodes in the alloy and 3×3 nodes in the walls ($I_p = 20, J_p = 128, I_w = 3, J_w = 3$, see §4.A), whence $\Delta r = 0.25 \text{ mm}$, $\Delta z = 0.7 \text{ mm}$, and $\Delta r_w = 1 \text{ mm}$, $\Delta z_w = 1 \text{ mm}$. The quartz properties values used are: $\rho^w = 2.203 \text{ g/cm}^3$, $c_p^w = 1.045 \text{ J/gK} = 0.2496 \text{ cal/g K}$, $k^w = 6.4 \times 10^{-3} \text{ cal/cm s K}$. The thermophysical properties of $(HgTe)_{1-x}(CdTe)_x$ used in this code are composition and temperature dependent, described in detail in [3], except for the density which is taken as constant $\rho \equiv 7.53 \text{ g/cm}^3$.

All nodes become constitutionally supercooled (mushy) by time $t = 10 \text{ s}$ and solidification begins at about that time. The alloy solidifies at $t = 110 \text{ s}$, with a sharp composition gradient near the lateral wall similar to that seen in the one-dimensional simulations described in [1], [15].

Sample output is shown in Table 1, produced at desired time intervals (specified by the user), for preselected columns ($i = 1, 5, 10, 15, 20$) and rows ($j = 1, 32, 64, 96, 128$); in addition, temperatures are shown at the inner-most and outer-most wall nodes (in top, bottom, and lateral walls). As computational checks, heat and mass balances are also shown. The phase index array (iphase) prints a 2 for liquid, 1 for mushy and 0 for solid, for all columns and preselected rows ($i = 1, 16, \dots, 128$) of the mesh. It serves as a convenient visualization of how the solidification progresses, see Table 2.

In addition to the standard output, composition and temperature histories of preselected nodes, as well as profiles of preselected rows at desired time-intervals may be produced. Examples are shown in Figures 3 and 4.

Table 1. Sample output from BAS-2D

```

*****
Time = 50.00(s) | no of steps= 2112 | Tbry= 650.00

liquid fractions: alam , every -32
.000000 .000000 .000000 .000000 .000000
.666819 .644573 .546565 .157008 .000000
.666819 .644573 .546565 .157008 .000000
.666819 .644573 .546565 .157008 .000000
.000000 .000000 .000000 .000000 .000000
mole fractions: j=Jp,1, -32
.204661 .204398 .203459 .201846 .205154
.197825 .197712 .197307 .198508 .211314
.197825 .197712 .197307 .198508 .211314
.197825 .197712 .197307 .198508 .211314
.204661 .204398 .203459 .201846 .205154
Temperatures: j=Jp,1, -32
653.333 653.101 652.419 651.527 650.632 650.457 650.086
667.164 665.841 662.245 657.641 653.228 652.461 650.461

680.993 677.981 671.286 662.940 655.261 653.835 650.691
741.495 739.115 729.967 708.546 670.768 664.028 652.408
741.495 739.115 729.967 708.546 670.768 664.028 652.408
741.495 739.115 729.967 708.546 670.768 664.028 652.408
680.993 677.981 671.286 662.940 655.261 653.835 650.691

667.164 665.841 662.245 657.641 653.228 652.461 650.461
653.333 653.101 652.419 651.527 650.632 650.457 650.086
iphase : j=Jp,1, -32 /2
00000000000000000000
11111111111111100000
11111111111111100000
11111111111111100000
11111111111111100000
11111111111111100000
11111111111111100000
11111111111111100000
11111111111111100000
00000000000000000000
Eold= -343.364945689206138 Enew= -343.542343164036083
Energy balance : 0.305228065045071162E-12
Mass balance :-0.333635796948783536E-03
latest time-step dt = 0.238355138087157671E-01
*****

```

Table 2. Phase array at various times (only every 16th row is shown)

time = 0	time = 40 sec
22222222222222222222	00000000000000000000
22222222222222222222	11111111111111111000
22222222222222222222	11111111111111111000
22222222222222222222	11111111111111111000
22222222222222222222	11111111111111111000
22222222222222222222	11111111111111111000
22222222222222222222	11111111111111111000
22222222222222222222	11111111111111111000
22222222222222222222	00000000000000000000
time = 5 sec	time = 60 sec
11111111111111111111	00000000000000000000
22222222222221111111	11111111111110000000
22222222222221111111	11111111111110000000
22222222222221111111	11111111111110000000
22222222222221111111	11111111111110000000
22222222222221111111	11111111111110000000
22222222222221111111	11111111111110000000
22222222222221111111	11111111111110000000
11111111111111111111	00000000000000000000
time = 10 sec	time = 100 sec
11111111111111111110	00000000000000000000
11111111111111111111	11111100000000000000
11111111111111111111	11111100000000000000
11111111111111111111	11111100000000000000
11111111111111111111	11111100000000000000
11111111111111111111	11111100000000000000
11111111111111111111	11111100000000000000
11111111111111111111	11111100000000000000
11111111111111111110	00000000000000000000
time = 20 sec	time = 109 sec
11111111111110000000	00000000000000000000
11111111111111111110	10000000000000000000
11111111111111111110	10000000000000000000
11111111111111111110	10000000000000000000
11111111111111111110	10000000000000000000
11111111111111111110	10000000000000000000
11111111111111111110	10000000000000000000
11111111111111111110	10000000000000000000
11111111111111111110	10000000000000000000
11111111111110000000	00000000000000000000

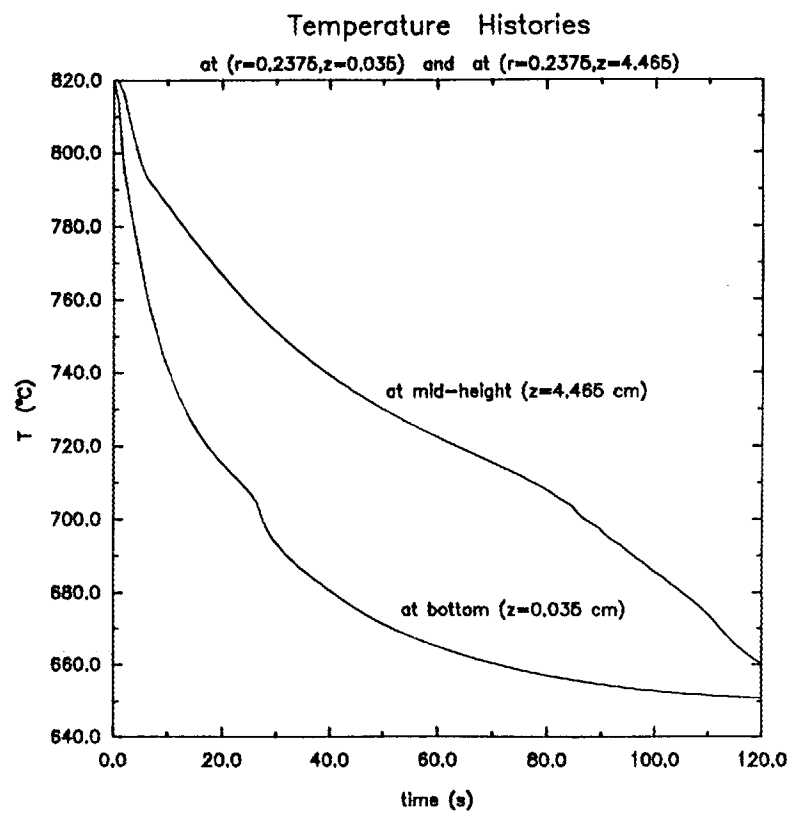
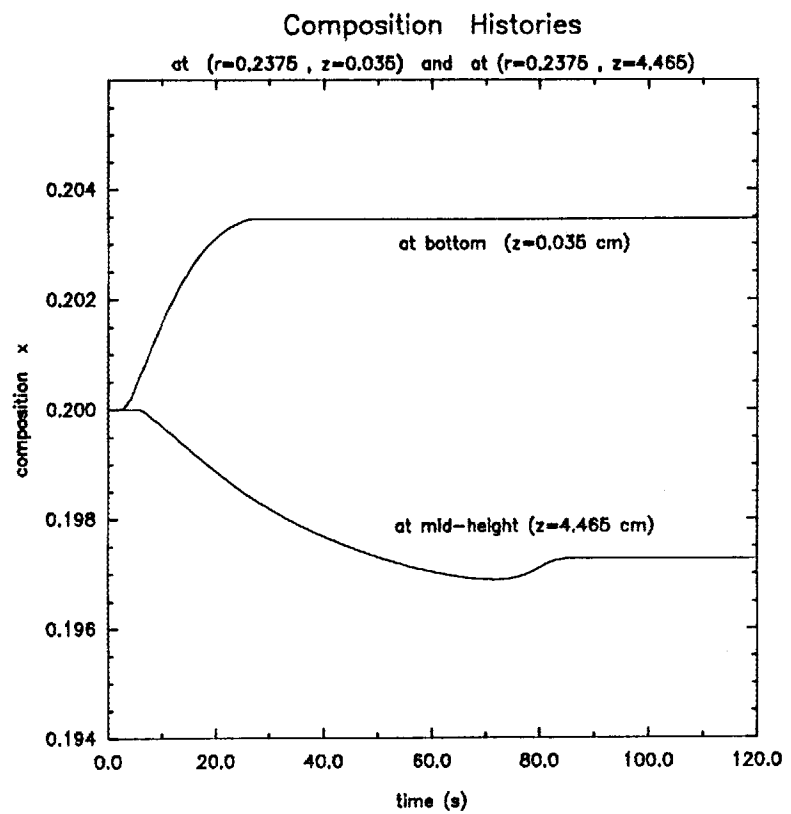


Figure 3

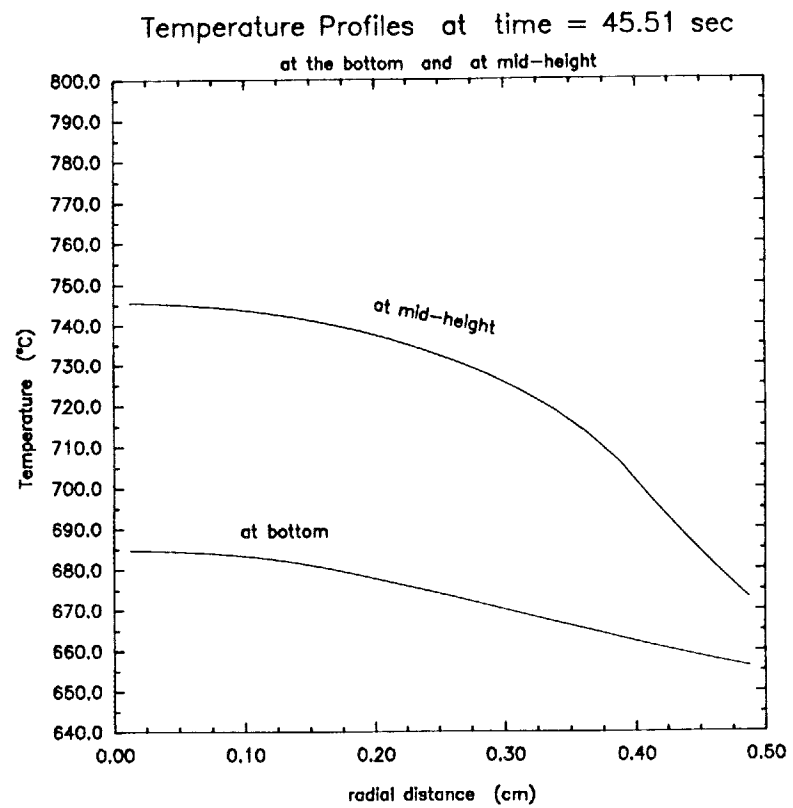
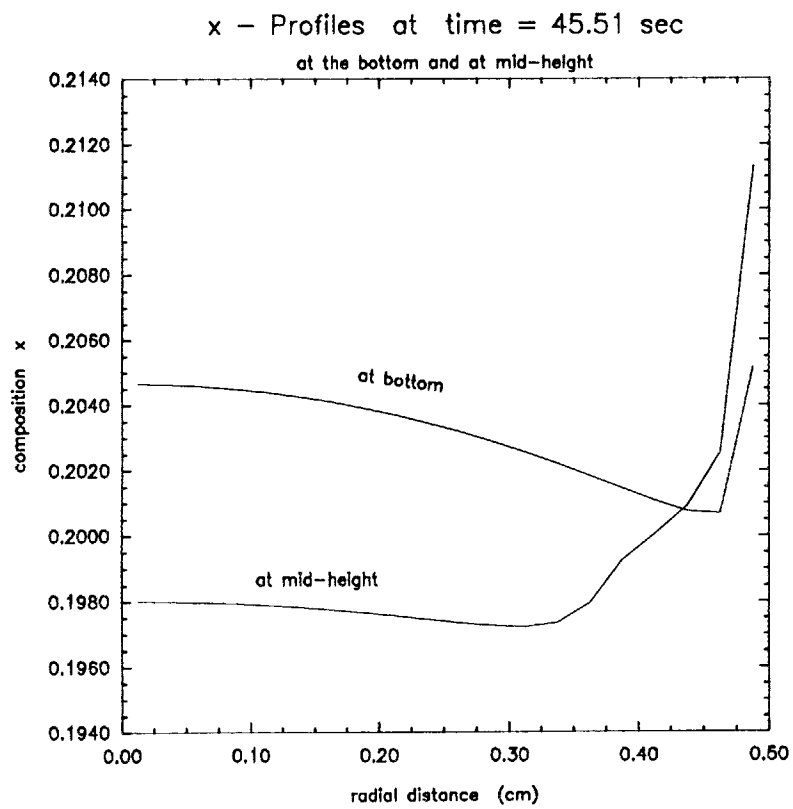


Figure 4 (a)

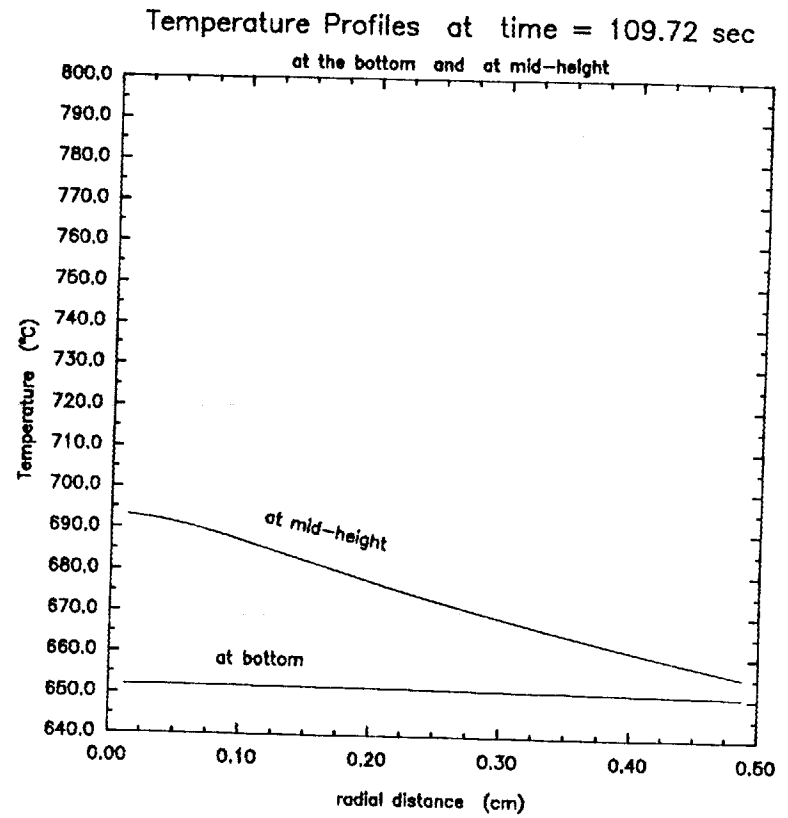
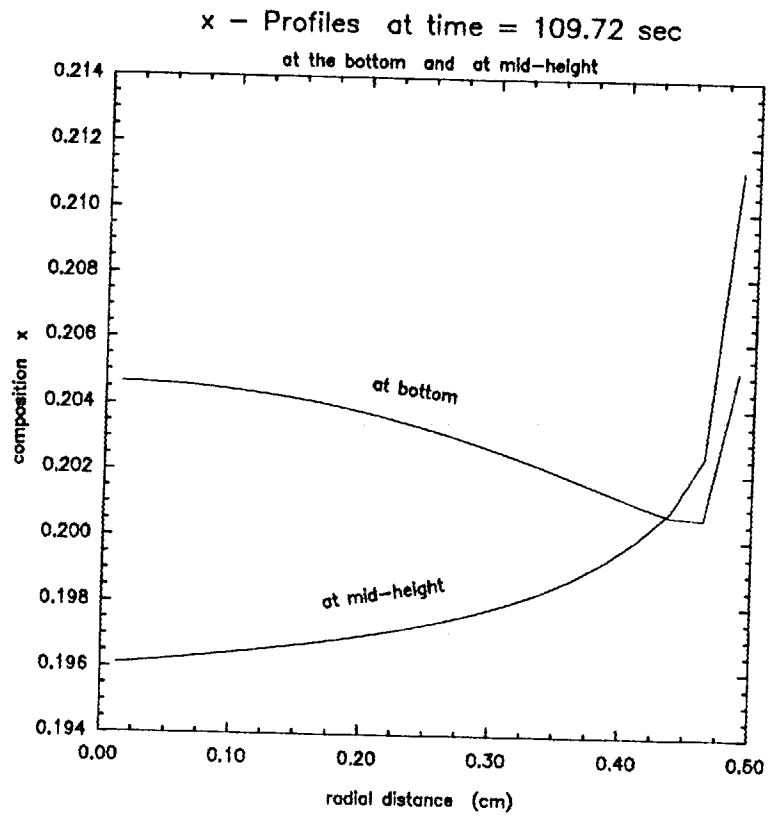


Figure 4 (b)

REFERENCES

- [1] Alexiades, V., G. A. Geist and A. D. Solomon, "Numerical Simulation of a $HgCdTe$ Solidification Process", Oak Ridge National Laboratory Report, ORNL-6127, August 1985.
- [2] Alexiades, V., D. G. Wilson, and A. D. Solomon, "Macroscopic global modeling of binary alloy solidification processes", *Quarterly Appl. Math.*, **43** (2) (1985), 143-158.
- [3] Alexiades, V., "Casting of $HgCdTe$, Part I: Thermophysical Property Values", Oak Ridge National Laboratory Report ORNL/TM-11734, 1991.
- [4] Alexiades, V., "Casting of $HgCdTe$, Part III: Numerical Experiments", Oak Ridge National Laboratory Report, to appear.
- [5] Bird, R. B., W. E. Stewart, and E. N. Lightfoot, *Transport Phenomena*, Wiley, 1960.
- [6] Brebrick, R. F., C.-H. Su and P.-K. Liao, "Associated Solution Model for $Ge-In-56$ and $Hg-Cd-Te$ ", pp. 171-253, in *Semiconductors and Semimetals*, eds R. K. Willardson and A. C. Beer, Academic Press, New York, 1983.
- [7] *Chemical Engineering Handbook*, McGraw-Hill, 1973.
- [8] Elliott, C. M. and J. R. Ockendon, *Weak and Variational Methods for Moving Boundary Problems*, Pitman, 1982.
- [9] Ladyzhenskaya, O. A., V. A. Solonikov, and N. N. Ural'tserva, *Linear and Quasilinear equations of parabolic type*, Amer. Math. Society, 1968.
- [10] Morris, M. D. and V. Alexiades, "Sensitivity Analysis of a Numerically simulated $HgCdTe$ solidification process by statistical methods", Oak Ridge National Laboratory Report, ORNL-6210, 1986.
- [11] Narang, H. N. and J. B. Drake, "Parallel solutions of a 2-D phase change problem on a Hypercube", Oak Ridge National Laboratory Report, ORNL-6504, 1989.
- [12] Nelson, D. A., Higgins, W. M., and Lancaster, R. A. "Advances in $(Hg, Cd)Te$ materials technology", *Proc. Soc. Photo-Optical Instrum. Eng.*, **225** (1980).
- [13] Press, W. H., B. P. Flannery, S. A. Teukolsky, W. T. Vetterling, *Numerical Recipes*, Cambridge University Press, 1986.
- [14] Su, C.-H., "Heat capacity, enthalpy of mixing, and thermal conductivity of $Hg_{1-x}Cd_xTe$ pseudobinary melts", *J. Crystal Growth*, **78** (1986), 51-77.
- [15] Su, C.-H., G. L. E. Perry, F. R. Szofran, and S. L. Lehoczky, "Compositional redistribution during casting of $Hg_{0.8}Cd_{0.2}Te$ alloys", *J. of Crystal Growth*, **91** (1988), 20-26.
- [16] Woods, M., *Thermodynamics of Fluid Systems*, Oxford University Press, 1975.

INTERNAL DISTRIBUTION

- | | | | |
|--------|-------------------------------------------------|--------|-------------------------------|
| 1-5. | V. Alexiades | 21. | R. P. Wichner |
| 6. | B. R. Appleton | 22. | Central Research Library |
| 7-8. | T. S. Darland/
Mathematical Sciences Library | 23. | K-25 Library |
| 9. | M. Olszewski | 24. | ORNL Patent Office |
| 10-14. | S. A. Raby | 25. | Y-12 Technical Library |
| 15. | J. J. Tomlinson | 26. | Laboratory Records - RC |
| 16-20. | R. C. Ward | 27-28. | Laboratory Records Department |

EXTERNAL DISTRIBUTION

29. Professor Roger W. Brockett, Wang Professor of Electrical Engineering and Computer Science, Division of Applied Sciences, Harvard University, Cambridge, MA 02138
30. Dr. John Cavallini, Acting Director, Scientific Computing Staff, Applied Mathematical Sciences, Office of Energy Research, U.S. Department of Energy, Washington, DC 20585
31. Dr. Alexandre Chorin, Mathematics Department, Lawrence Berkeley Laboratory, Berkeley, CA 94720
32. Dr. James Coronas, Ames Laboratory, Iowa State University, Ames, IA 50011
33. Dr. John J. Dorning, Department of Nuclear Engineering Physics, Thornton Hall, McCormick Road, University of Virginia, Charlottesville, VA 22901
34. Professor Richard E. Ewing, Department of Mathematics, University of Wyoming, Laramie, WY 82071
35. Professor James Glimm, Department of Mathematics, State University of New York, Stony Brook, NY 11794
36. Dr. Hans Kaper, Mathematics and Computer Science Division, Argonne National Laboratory, 9700 S. Cass Avenue, Argonne, IL 60439
37. Professor Peter D. Lax, Courant Institute of Mathematical Sciences, New York University, 251 Mercer Street, New York, NY 10012
38. Dr. Alex Lehoczky, ES 72, Space Science Laboratory, Marshall Space Flight Center, NASA, Huntsville, AL 35812

39. Dr. James E. Leiss, 13013 Chestnut Oak Drive, Gaithersburg, MD 20878
40. Professor Neville Moray, Department of Mechanical and Industrial Engineering, University of Illinois, 1206 West Green Street, Urbana, IL 61801
41. Lee Riedinger, Director, The Science Alliance Program, University of Tennessee, Knoxville, TN 37996
42. Dr. Alan Solomon, 90 Eshel St., P.O. Box 227, Omer 84965, Israel
43. Dr. Chin-Hua Su, ES 72, Space Science Laboratory, Marshall Space Flight Center, NASA, Huntsville, AL 35812
44. Dr. Frank Szofran, ES 72, Space Science Laboratory, Marshall Space Flight Center, NASA, Huntsville, AL 35812
45. Professor Mary F. Wheeler, Department of Mathematical Sciences, Rice University, P.O. Box 1892, Houston, TX 77251
46. Office of Assistant Manager for Energy Research and Development, U.S. Department of Energy, Oak Ridge Operations Office, P.O. Box 2001, Oak Ridge, TN 37831-8600
- 47-56. Office of Scientific and Technical Information, P. O. Box 62, Oak Ridge, TN 37830